Chinese Journal of Chemistry, **2009**, *27*, 472—478 **Full Paper**

Molecular Simulation Study of Hexane Diffusion in Dynamic Metal-Organic Frameworks

XUE, Chunyu(薛春瑜) ZHONG, Chongli(仲崇立)

Laboratory of Computational Chemistry, Department of Chemical Engineering, Beijing University of Chemical Technology, Beijing 100029, China

The modified MM3 force field for describing flexible IRMOF-1 was extended to include other IRMOFs, and a molecular dynamics simulation study was performed on hexane diffusion in IRMOF-1 and IRMOF-16. The self-diffusion coefficients and diffusion pathways of hexane, as well as the mobility of the frameworks were investigated, as a function of both temperature and loading. The results revealed that the diffusion pathway of hexane was largely influenced by loading, and the flexibility of IRMOF-16 was much larger than that of IRMOF-1. The microscopic information obtained is useful for understanding the diffusion mechanism of chain molecules in dynamic MOF.

Keywords diffusion, chain molecule, molecular simulation, flexibility, metal-organic framework

Introduction

Metal-organic frameworks (MOF), as a class of new nanoporous materials, have received much attention due to their potential applications to gas storage, separation, catalysis, *etc*.[1-7] In most applications, such as storage and separation processes, knowledge of both gas adsorption and diffusion is required but so far the studies focused on the adsorption behavior, both experimentally[8-12] and theoretically,[13-28] and investigations on gas diffusion in MOF are very scarce. There are only a couple of experimental studies to date on gas diffusion in MOF.[29-31] Although several theoretical studies have been performed on diffusion in MOF, most of them[32-36] treated the framework as rigid; furthermore, such treatments could not include the impact of flexibility on diffusion. As a result, several efforts have been made very recently to take into account the flexibility of MOF by developing new force fields that can describe the dynamics of the MOF.[37-40] Greathouse *et al*.[37] developed a new force field for IRMOF-1 based on the CVFF,[41] and found that the structure of IRMOF-1 collapsed at higher water contents by molecular dynamics (MD) simulation, which is consistent with the experimental observations.[42] Huang *et al*.[39] proposed a force field for IRMOF-1 with basic potential functions based on *ab initio* calculations, and investigated the thermal conductivity of IRMOF-1. Tafipolsky *et al*.,[40] on the other hand, extended the MM3 force field[43] to IRMOF-1 based on *ab initio* calculations. Using the new force fields developed, there were three MD simulations performed on the diffusion in dynamic MOF, *i.e*., the self-diffusivity of benzene in IRMOF-1 was investigated by Amirjalayer *et al*.[44]; Dubbeldam *et al*.[38] improved the CVFF modified by Greathouse *et al*.,[37] and performed MD simulations on benzene diffusion in IRMOF-1; in recently, Greathouse *et al*.[45] calculated the benzene diffusivity in IRMOF-1 using their modified CVFF.

Obviously, the studies on diffusion in dynamic MOF are very scarce to date, and thus the knowledge on the influence of framework flexibility on diffusion, and vice versa, is very limited. Therefore, this work performed a systematic study on chain molecule diffusion in dynamic MOF, in which the diffusion of hexane in two IRMOFs, IRMOF-1 and -16, was adopted as an example. This work firstly extended the MM3 force field modified by Tafipolsky *et al*.[40] for IRMOF-1 to other IRMOFs, IRMOF-10, IRMOF-14, and IRMOF-16. Then, the diffusion mechanisms as well as the framework flexibility were discussed in details by performing MD simulations on hexane diffusion in IRMOF-1 and -16 at 300 and 450 K.

Models and simulation method

MOF structure

The crystal structure of IRMOF is very simple which consists of Zn_4O clusters and various linkers to form a three-dimensional porous cubic framework. Figure 1 shows the crystal structures of the IRMOF with different linkers studied in this work. Details can be found elsewhere.

Simulation details

In this work, all MD simulations were performed with the TINKER program package. The NVT ensem-

* E-mail: zhongcl@mail.buct.edu.cn; Tel.: 0086-010-64419862.
Receibed April 16, 2008; revised August 27, 2008; accepted November 22, 2008.
Project supported by the National Science Foundation for Distinguished Young Scholars of China (No. 20725622).

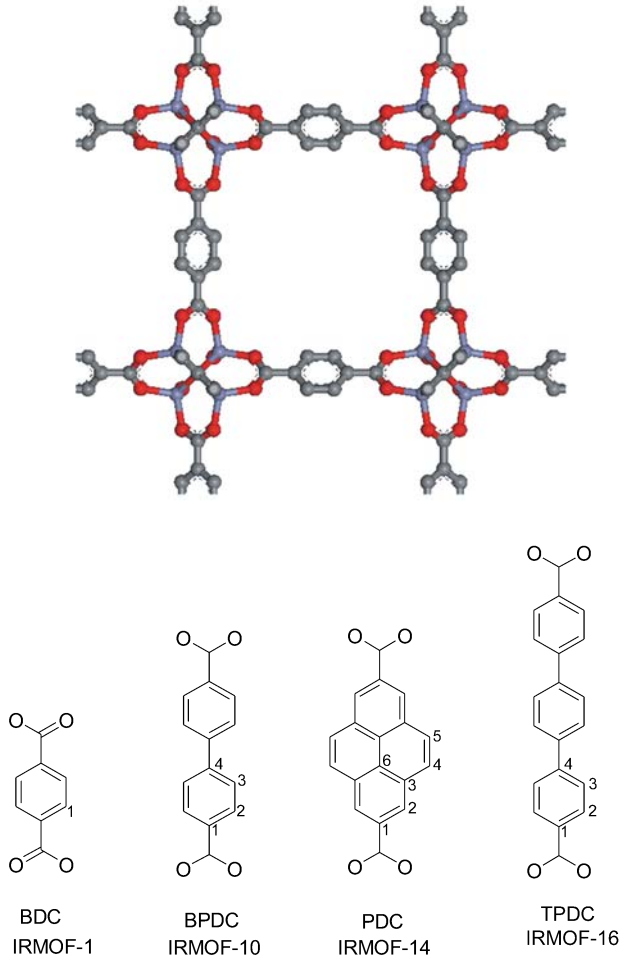

Figure 1 Unit cell crystal structure of IRMOF with different linkers.

ble was used to investigate loading dependency of self-diffusivities of hexane in IRMOF-1 and -16 at 300 and 450 K, in which temperature was held constant by Berendsen thermostat. The simulation cell consisted of $1\times1\times1$ to $2\times2\times2$ elementary cells of the IRMOF crystal lattice. MD simulations with modified Beeman propagator consisted of 5×10^5 steps to guarantee the equilibration for the system followed by 2.5×10^6 steps to sample the diffusion properties of interest. The time-step was taken as 1 fs and a configuration was stored every 0.1 ps. Thus, a total of 25000 configurations per trajectory were stored and used for the further analysis. We have performed 10 independent MD simulations for each loading. From the 25000 stored configurations of each trajectory, the self-diffusion coefficient D_s was calculated by the mean square particle displacement (MSD) method in the range of time intervals from 250 to 1000 ps. The probability density was generated from the center of mass (COM) trajectories of 25000 stored configurations with a grid of 1.297 Å of the unit cell and was analyzed and rendered with the program XcrysDen. The trajectory of an isolated hexane molecule was plotted according to the configurations selected at 30 intervals from the total of 25000 ones.

Results and discussion

Validation of the method

To validate our method, constant-temperature equilibrium MD simulations were performed to calculate the self-diffusivities of benzene in IRMOF-1. To compare with the simulation results obtained by Amirjalayer *et al.*,[44] the system was selected to contain 10 benzene molecules per unit cell of IRMOF-1. The results in Figure 2 show that our simulation reproduces well their results.[44] Furthermore, the contour plots of the COM probability density in planes shown in Figure 3 are also nearly identical to those obtained by them.[44]

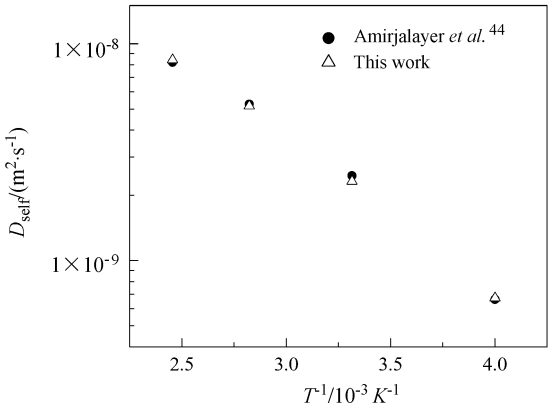

Figure 2 Comparison of simulated self-diffusivities of benzene in IRMOF-1.

Force fields

Extension of the MM3 force field for IRMOF Tafipolsky *et al.*[40] have extended the MM3 force filed to IRMOF-1. In this work, it was further extended to other IRMOFs (IRMOF-10, IRMOF-14 and IRMOF-16) based on *ab initio* calculations. Details of our method are given in the following.

(1) To obtain the force field parameters for the atoms involved in the IRMOF-10, -14, and -16, self-consistent field molecular orbital calculations were performed for the π-system using the modified Parser-Parr-Pople method as implemented in TINKER. Not only the values for the C—C bond stretching and the corresponding reference bond length, but also the twofold torsional parameters for the rotation around C—C bonds were refined.

(2) For IRMOF-10 and -16, the parameters of C(1), C(2) and C(3) (see Figure 1) are similar, and thus they were defined as one type of carbon atom in the extended force field and denoted as C(ph). The carbons (C(4)) located on conjugation positions are different from the C(ph) and marked as C(conj) for discrimination.

(3) The torsional parameters of C_6H_4 units were refined according to the torsional barriers for biphenyl. To describe the torsional potential of the C_6H_4 units, we used a single cosine term of the form $V(\varphi)=1/2V_0[1-\cos(2\varphi)]$, where φ is the C(ph)-C(conj)-C(conj)-C(ph)

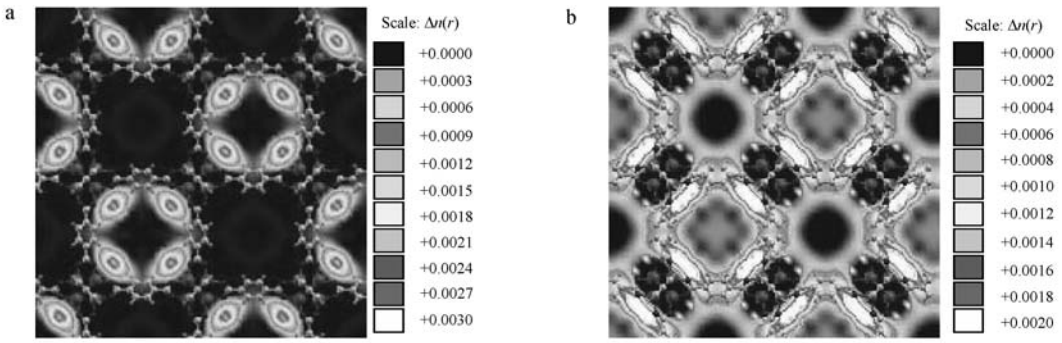

Figure 3 Plots of the COM probability density in planes a) through the maxima of the Zn_4O clusters and, b) through the cell centers.

dihedral angle and the parameter V_2 was adjusted to reproduce the barrier to internal rotation of the C_6H_4 units.

(4) With respect to IRMOF-14, it was found that the calculated lattice parameters with the new torsional parameters obtained in step (1) were very close to the values with those parameters in IRMOF-1. Thus, for simplicity, the torsional parameters in IRMOF-1 were also adopted in IRMOF-14.

(5) All the other parameters were taken from the work of Tafipolsky *et al*.[40]

The parameters obtained in this work are listed in Table 1, which were used to optimize the crystal structures of the IRMOF to validate their suitability. The calculated values of the lattice constants agree quite well with the experimental observations as shown in Table 2, illustrating that the parameters obtained are credible.

Force field for hexane As to hexane molecules, all-atom models were used and the parameters were taken from the original MM3 force field.[43] For the calculation of cross non-bonded interactions, the Lorenz-Berthelot mixing rules, with geometric averaging for $\sigma_{ij}=(\sigma_i+\sigma_j)/2$ and arithmetic averaging for $\varepsilon_{ij}=k_{ij}(\varepsilon_i\varepsilon_j)^{1/2}$, were adopted.

Self-diffusivities of hexane in IRMOF-1 and -16

In this work, the self-diffusion coefficients of hexane in two IRMOFs, IRMOF-1 and -16, were simulated at 300 and 450 K, respectively, as a function of loading. The results are shown in Figure 4a. At the loading of 10 molecules/UC and 300 K, our simulation gave a value of 2.017 10^{-9} $m^2 \cdot s^{-1}$for the self-diffusion coefficient of hexane in IRMOF-1, agreeing quite well with the experimental value[27] of $3.2\times10^{-9}-4.1\times10^{-9}$ $m^2 \cdot s^{-1}$ under similar conditions. From Figure 4a, it is evident that the self-diffusivity of hexane in IRMOF-1 is much slower than that in IRMOF-16, attributed mainly to the relatively smaller pore size in the former since they have similar pore topology and chemistry. In both the IRMOFs, the self-diffusivity of hexane increases with increasing temperature; however, the behavior is different within the loading range studied. In Figure 4b, the mean square displacement (MSD) curves (averaged

Table 1 Force field parameters obtained in this work

IRMOF	Bond stretching			Torsional parameters/(kJ•mol^{-1})	
	Types	Distance/nm	Force/(mdyn•nm^{-1})		
IRMOF-10	C(ph)—C(ph)	0.138	65.6	C(ph)-C(conj)-C(conj)-C(ph)	16.7
	C(ph)—C(conj)	0.139	65.0		
	C(ph)—C(conj)	0.146	53.9		
IRMOF-14	C(1)—C(2)	0.136	65.7		
	C(2)—C(3)	0.140	64.4		
	C(3)—C(4)	0.143	58.2		
	C(4)—C(5)	0.136	70.9		
	C(5)—C(6)	0.141	62.6		
	C(6)—C(6)	0.142	59.9		
IRMOF-16	C(ph)—C(ph)	0.138	65.6	C(ph)-C(conj)-C(conj)-C(ph)	16.7
	C(ph)—C(conj)	0.139	65.0		
	C(ph)—C(conj)	0.146	53.9		

Table 2 Comparison of the lattice constants of the IRMOF

Structure	Experiment *L*/nm	This work *L*/nm
IRMOF-10	3.4281[a,b]	3.4590
IRMOF-14	3.4381[a,b]	3.4283
IRMOF-16	4.2981[a,c]	4.3160

[a] The experimental values were taken from Eddaoudi *et al.*[46] [b] The space group is *Fm*3(*m*) for IRMOF-10 and 14. [c]The primitive cubic space group is *Pm*3(*m*) for IRMOF-16 doubled for comparisons.

over multiple time origins) of the hexane COM over the corresponding time intervals Δt are given for flexible models at the loading of 10/UC and 300 K in IRMOF-1, which is similar to benzene in IRMOF-1.[44]

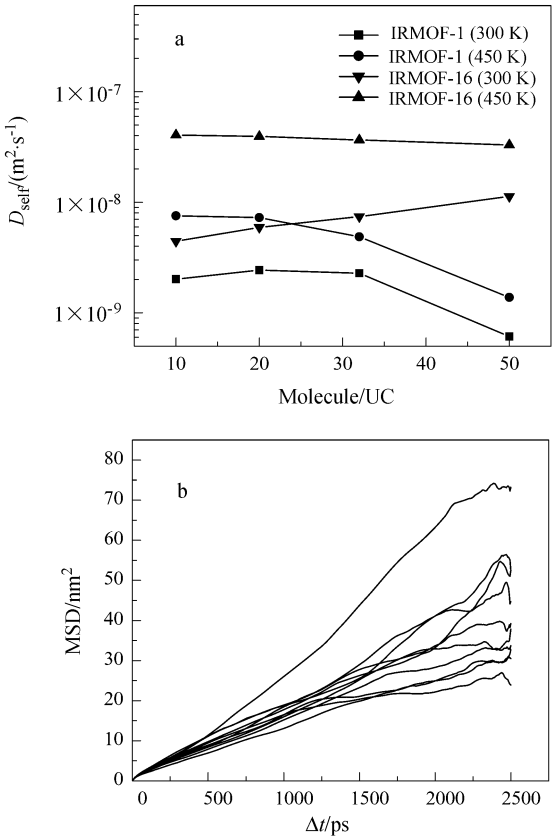

Figure 4 (a) Self-diffusivities of hexane in IRMOF-1 and -16 as a function of loading and (b) MSD curves with respect to time interval Δt at 300 K for a flexible lattice.

For IRMOF-1 at 300 K, the self-diffusivity of hexane first increases with increasing loading, followed by a decrease with the further increase of loading. This behavior has been observed for hydrogen diffusion in IRMOF,[33] which can be explained as that at lower loadings, the rate-limiting step for diffusion of hexane in IRMOF-1 is predominant, and the presence of nearby hexane reduces this energetic barrier through a cooperative effect and enhances the diffusivity, leading to a slight increase of self-diffusivity in a low concentration range; with increasing loading, steric hindrance effects become more obvious, and predominant eventually, resulting in a lowering of the hexane self-diffusivity. At 450 K, it is easier to overcome the energetic barrier to diffusion and thus steric hindrance effects are predominant influencing factors both at low and high loadings, resulting in a monotonous decreasing of hexane diffusion in IRMOF-1 as shown in Figure 4a. As for IRMOF-16, the diffusion behavior is similar to that in IRMOF-1. Since the pore size of IRMOF-16 is much larger, the concentration is far from saturation in the loading range studied, thus the self-diffusivity of hexane slightly increases at 300 K while decreases at 450 K in the loading range studied; we can observe the further decreasing trend of self-diffusivity in IRMOF-16 with further increasing loadings.

Diffusion mechanism

It is useful to understand the diffusion mechanism of chain molecules in MOF. Therefore, the COM probability distribution of hexane as well as the diffusion trajectories of an isolated hexane were calculated to give insight into molecular-level details of the underlying mechanisms. Details are given in the following paragraphs.

Center of mass probability distribution Figure 5 shows the COM probability distribution of hexane in IRMOF-1 at 300 K, in which the pores with the phenylene ring planes facing inside were labeled A, and the others B. According to Figure 5a, the molecules mainly accumulate just above the faces of the Zn_4O clusters of the A-pores at lower concentrations. When the concentration increases, the resident molecules in a B-pore increase. As shown in Figure 5c, hexane is unable to be close to the Zn_4O clusters in B-pores, attributed to the steric hindrance effect caused by the phenylene ring planes and the large size of hexane. As can be seen from Figures 5d—5f, the probability of the resident molecules firstly increases in the region of B-pore diagonal with increasing concentration; however, with the further increase of concentration, although the B-pores are occupied more and more by the molecules, the probability of the resident molecules in the region of B-pore diagonal decreases due to the steric hindrance effect.

Figure 6 shows the COM probability distribution of hexane in IRMOF-16 at 300 K. The molecules mainly accumulate just above the faces of the Zn_4O clusters at low concentrations, similar to that in IMROF-1. With further increasing the concentration, the molecules also occupied the region around the phenylene rings, the less preferential adsorption sites in IRMOF-16.

The quantitative relationships between the probability of resident molecules in an A-pore of IRMOF-1 and loading at 300 and 450 K are shown in Figure 7. Obviously, the probability of resident molecules in an A-pore decreases with increasing loading, to a value of *ca*. 65% when the concentration approaches saturation. This value is quite close to the ratio of the available volumes

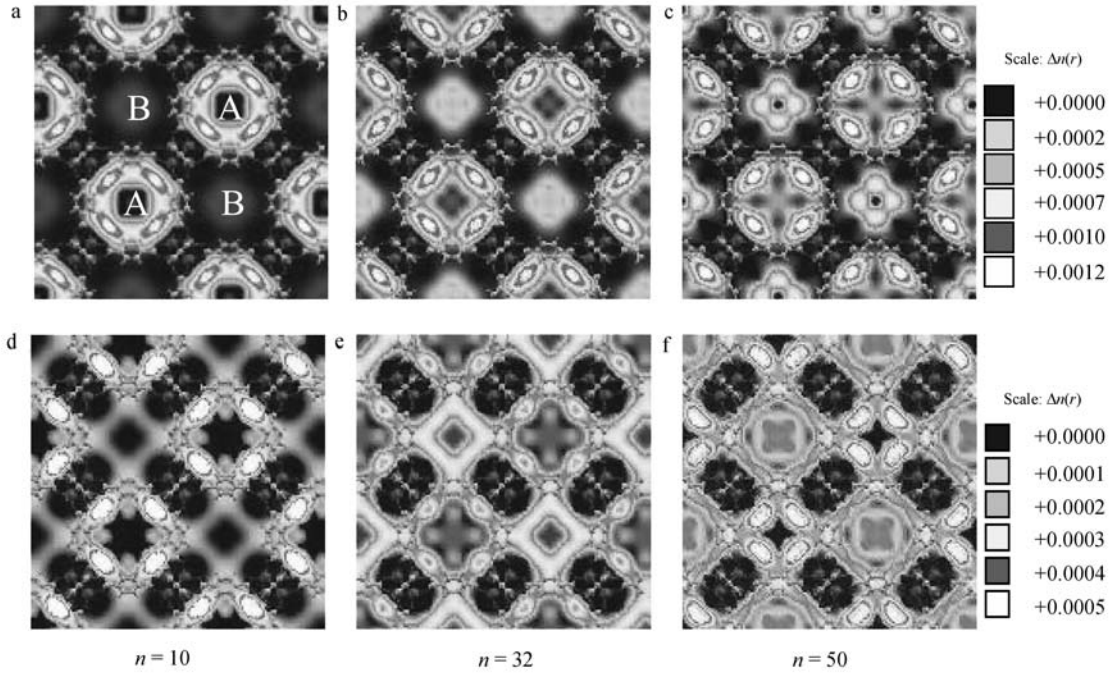

Figure 5 Plots of COM probability density in planes a—c through the maxima of the Zn_4O clusters and d—f through the pore centers at 300 K in IRMOF-1.

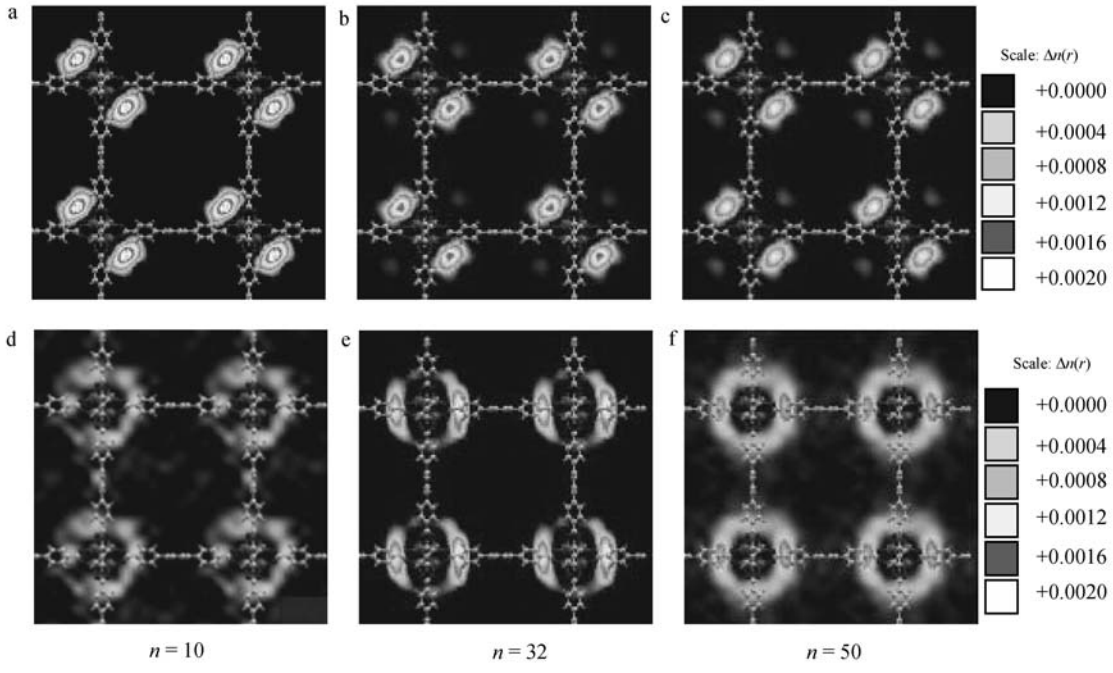

Figure 6 Plots of COM probability density in planes a—c through the maxima of the Zn_4O clusters and d—f through the cell centers at 300 K in IRMOF-16.

of A-pores to B-pores (pore diameter ratio: 14.3/10.9) in IRMOF-1. On the other hand, the higher the temperature, the smaller the probability of resident molecules in an A-pore at a concentration apart from saturation.

Diffusion trajectory of an isolated hexane molecule To study the diffusion pathway of hexane in MOF, the diffusion trajectories of an isolated hexane at 300 K in IRMOF-1 at various concentrations were further studied and the results are shown in Figure 8. For each loading the trajectories of more than 30 molecules with different initial velocities were examined to obtain credible pathways. Generally, there are two kinds of diffusions in IRMOF-1: one is the short-distance diffusion within a pore, and the other is the so-called long-distance diffusion, that is the inter-pore diffusion. After an examination of the trajectories shown in Figure 8 and

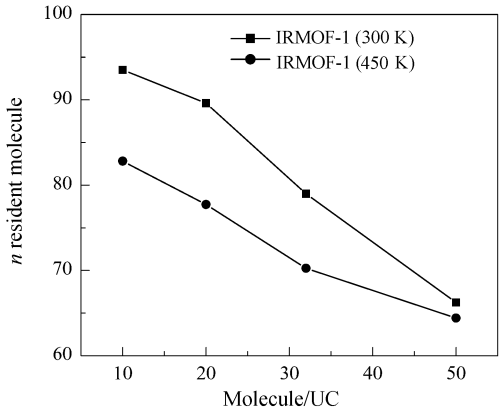

Figure 7 Probability of resident molecules in an A-pore of IRMOF-1 versus loading.

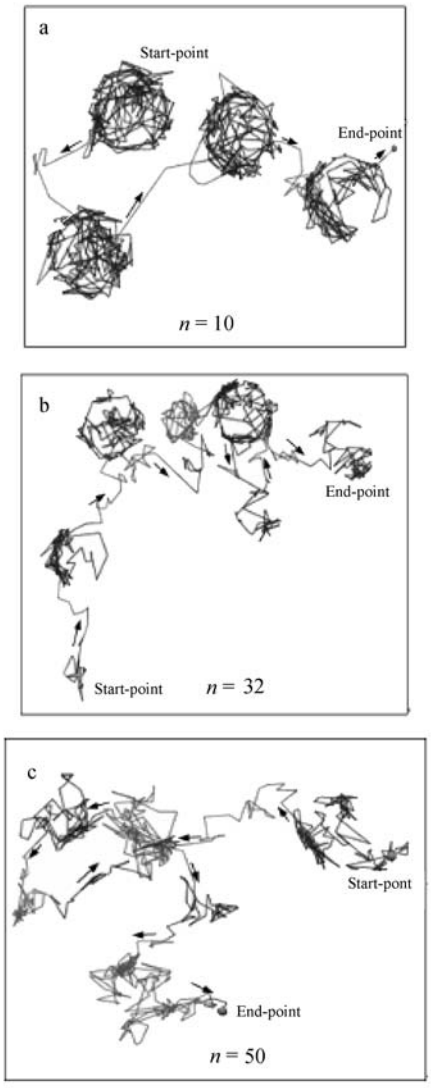

Figure 8 Diffusion trajectories of an isolated hexane molecule in IRMOF-1 at 300 K with various loadings.

the COM probability distributions (Figure 5), we proposed the following mechanism for hexane diffusion in IRMOF-1: at lower concentrations, the intra-pore (short-distance) diffusion is predominant, and a hexane molecule mainly diffuses in A-pores and passes a B-pore quickly to another A-pore; with increasing concentration, the diffusion time of a hexane molecule in B-pores increases, and it becomes easier for hexane to diffuse from one A-pore to another A-pore through the center of the connecting windows since the presence of nearby hexane reduces the energetic barrier to across the pores; at even higher concentrations, the pathway from one A-pore to another A-pore becomes less favorable because of the steric hindrance effect caused by the increment of resident molecules in B-pores. In this case, hexane inclines to have intra-pore diffusion, both in A- and B-pores. As for hexane in IRMOF-16, the diffusion pathway is simply from one Zn_4O cluster to another one along the phenylene ring in the loading range studied, and thus the trajectories of isolated hexane molecules were omitted.

Mobility of linkers

The amplitude of linkers in an MOF can reflect the flexibility of the MOF. Therefore, the amplitudes of the phenylene rings in both IRMOF-1 and -16 were calculated, as a function of both temperature and loading as shown in Figure 9. Obviously, the amplitude of the phenylene ring in IRMOF-16 is much larger than that in IRMOF-1, illustrating that the flexibility of the former is much larger than that of the latter. Compared with the influence of loading, which is negligible in the range studied, the effect of temperature is much more significant.

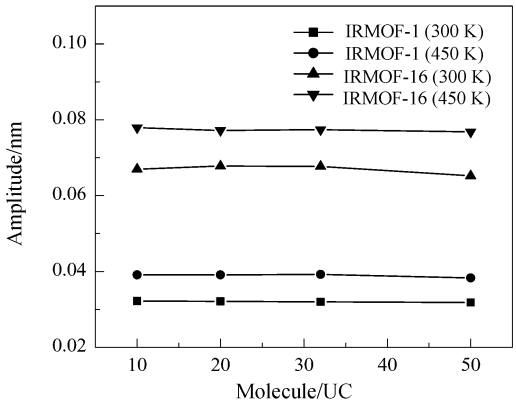

Figure 9 Amplitudes of the phenylene rings in IRMOF-1 and -16.

Conclusion

This work shows that the diffusion pathway of chain molecules in MOF may be largely affected by loading, depending on the structure of the pores. For systems with weak guest-host interactions, the effect of loading on framework flexibility is insignificant, while the influence of temperature is much more evident. Based on the simulation results, it is clear that the flexibility of the framework of IRMOF-16 is much larger than that of IRMOF-1, attributed mainly to the difference in the nature of the organic linkers. The extended force field is

useful for doing comparative studies for IRMOF to provide a comprehensive understanding of guest adsorption and diffusion in dynamic MOF, leading to a better application of MOF to industry.

References

1 Snurr, R. Q.; Hupp, J. T.; Nguyen, S. T. *AIChE J*. **2004**, *50*, 1090.
2 Schlichte, K.; Kratzke, T.; Kaskel, S. *Microporous Mesoporous Mater*. **2004**, *73*, 81.
3 Pan, L.; Adams, K. M.; Hernandez, H. E.; Wang, X.; Zheng, C.; Hattori, Y.; Kaneko, K. *J. Am. Chem. Soc*. **2003**, *125*, 3062.
4 Ohmori, O.; Kawano, M.; Fujita, M. *Angew. Chem., Int. Ed*. **2005**, *44*, 1962.
5 Dybtsev, D. N.; Chun, H. C.; Yoon, S. H.; Kim, D.; Kim, K. *J. Am. Chem. Soc*. **2004**, *126*, 32.
6 Fletcher, A. J.; Cussen, E. J.; Bradshaw, D.; Rosseinsky, M. J.; Thomas, K. M. *J. Am. Chem. Soc*. **2004**, *126*, 9750.
7 Rowsell, J. L. C.; Yaghi, O. M. *Angew. Chem., Int. Ed*. **2005**, *44*, 4670.
8 Rosi, N. L.; Eckert, J.; Eddaoudi, M.; Vodak, D. T.; Kim, J.; O'Keeffe, M.; Yaghi, O. M. *Science* **2003**, *300*, 1127.
9 Kubota, Y.; Takata, M.; Matsuda, R.; Kitaura, R.; Kitagawa, S.; Kato, K.; Sakata, M.; Kobayashi, T. C. *Angew. Chem., Int. Ed*. **2005**, *44*, 920.
10 Kesanli, B.; Cui, Y.; Smith, M. R.; Bittner, E. W.; Bockrath, B. C.; Lin, W. *Angew. Chem., Int. Ed*. **2005**, *44*, 72.
11 Dincă, M.; Long, J. R. *J. Am. Chem. Soc*. **2005**, *127*, 9376.
12 Li, Y.; Yang, R. *J. Am. Chem. Soc*. **2006**, *128*, 726.
13 Sagara, T.; Klassen, J.; Ortony, J.; Ganz, E. *J. Chem. Phys*. **2005**, *123*, 14701.
14 Mueller, T.; Ceder, G. *J. Phys. Chem. B* **2005**, *109*, 17974.
15 Bordiga, S.; Vitillo, J. G.; Ricchiardi, G.; Regli, L.; Cocina, D.; Zecchina, A.; Arstad, B.; Bjørgen, M.; Hafizovic, J.; Lillerud, K. P. *J. Phys. Chem. B* **2005**, *109*, 18237.
16 Yildirim, T.; Hartman, M. R. *Phys. Rev. Lett*. **2005**, *95*, 215504.
17 Garberoglio, G.; Skoulidas, A. I.; Johnson, J. K. *J. Phys. Chem. B* **2005**, *109*, 13094.
18 Yang, Q.; Zhong, C. *J. Phys. Chem. B* **2006**, *110*, 655.
19 Yang, Q; Zhong, C. *J. Phys. Chem. B* **2006**, *110*, 17776.
20 Jung, D. H.; Kim, D.; Lee, T. B.; Choi, S. B.; Yoon, J. H.; Kim, J.; Choi, K.; Choi, S.-H. *J. Phys. Chem. B* **2006**, *110*, 22987.
21 Zhang, L.; Wang, Q.; Liu, Y.-C. *Chem. Eur. J*. **2007**, *13*, 6387.
22 Düren, T.; Snurr, R. Q. *J. Phys. Chem. B* **2004**, *108*, 15703.
23 Vishnyakov, A.; Ravikovitch, P. I.; Neimark, A. V.; Bülow, M.; Wang, Q. M. *Nano Lett*. **2003**, *3*, 713.
24 Yang, Q.; Xue, C.; Zhong, C.; Chen, J. *AIChE J*. **2007**, *53*, 2832.
25 Han, S. S; Goddard III, W. A. *J. Am. Chem. Soc*. **2007**, *129*, 8422.
26 Han, S. S.; Deng, W-Q.; Goddard III, W. A. *Angew. Chem., Int. Ed*. **2007**, *46*, 6289.
27 Wang, S.; Yang, Q.; Zhong, C. *Acta Chim. Sinica* **2006**, *64*, 1775 (in Chinese).
28 Wang, S.; Zhong, C. *Acta Chim. Sinica* **2006**, *64*, 2375 (in Chinese).
29 Stallmach, F.; Gröger, S.; Künzel, V.; Kärger, J.; Yaghi, O. M.; Hesse, M.; Müller, U. *Angew. Chem., Int. Ed*. **2006**, *45*, 2123.
30 Kortunov, P. V.; Heinke, L.; Arnold, M.; Nedellec, Y.; Jones, D. J.; Caro, J.; Karger, J. *J. Am. Chem. Soc*. **2007**, *129*, 8041.
31 Salles, F.; Jobic, H.; Maurin, G.; Koza, M. M.; Llewellyn, P. L.; Devic, T.; Serre, C.; Ferey, G. *Phys. Rev. Lett*. **2008**, *100*, 245901.
32 Skoulidas, A. I.; Sholl, D. S. *J. Phys. Chem. B* **2005**, *109*, 15760.
33 Yang, Q.; Zhong, C. *J. Phys. Chem. B* **2005**, *109*, 11862.
34 Skoulidas, A. I. *J. Am. Chem. Soc*. **2004**, *126*, 1356.
35 Keskin, S.; Sholl, D. S. *J. Phys. Chem. C* **2007**, *110*, 14055.
36 Sarkisov, L.; Duren, T.; Snurr, R. Q. *Mol. Phys*. **2004**, *102*, 211.
37 Greathouse, J.; Allendorf, M. *J. Am. Chem. Soc*. **2006**, *128*, 10678.
38 Dubbeldam, D.; Walton, K. S.; Ellis, D. E.; Snurr, R. Q. *Angew. Chem., Int. Ed*. **2007**, *46*, 4496.
39 Huang, B.; McGaughey, A. J. H.; Kaviany, M. *J. Heat. Mass. Tranfer*. **2007**, *50*, 393.
40 Tafipolsky, M.; Amirjalayer, S.; Schmid, R. *J. Comput. Chem*. **2007**, *28*, 1169.
41 Dauber-Osguthorpe, P.; Roberts, V. A.; Osguthorpe, D. J.; Wolff, J.; Genest, M.; Hagler, A. T. *Proteins*: *Struct. Funct. Genet*. **1988**, *4*, 31.
42 Huang, L. M.; Wang, H. T.; Chen, J. X.; Wang, Z. B.; Sun, J. Y.; Zhao, D. Y.; Yan, Y. S. *Microporous Mesoporous Mater*. **2003**, *58*, 105.
43 Li, J.-H.; Allinger, N. L.; Yuh, Y. H. *J. Am. Chem. Soc*. **1989**, *111*, 8551.
44 Amirjalayer, S.; Tafipolsky, M.; Schmid, R. *Angew. Chem., Int. Ed*. **2006**, *45*, 463.
45 Greathouse, J. A.; Allendorf, M. D. *J. Phys. Chem. C* **2008**, *112*, 5795.
46 Eddaoudi, M.; Kim, J.; Rosi, N.; Vodak, D.; Wachter, J.; O'Keeffe, M.; Yaghi, O. M. *Science* **2002**, *295*, 469.
47 Ponder, J. W.; Richards, F. M. *J. Comput. Chem*. **1987**, *8*, 1016.
48 Berendsen, H. J. C.; Postma, J. P. M.; van Gunsteren, W. F.; DiNola, A.; Haak, J. R. *J. Chem. Phys*. **1984**, *81*, 3684.
49 Beeman, D. *J. Comput. Phys*. **1976**, *20*, 130.
50 Kakalj, A. *Comp. Mater. Sci*. **2003**, *28*, 155.
51 Arulmozhiraja, S.; Fujii, T. *J. Chem. Phys*. **2001**, *115*, 10589.

(E0804161 Zhao, X.)